Validating satellite derived and modelled sea-ice drift in the Laptev Sea with in situ measurements from the winter of 2007/08

Polona Rozman,[1] Jens A. Hölemann,[2] Thomas Krumpen,[1] Rüdiger Gerdes,[1] Cornelia Köberle,[1] Thomas Lavergne,[3] Susanne Adams[4] & Fanny Girard-Ardhuin[5]

1 Sea Ice Physics, Alfred Wegener Institute for Polar and Marine and Research, Bussestr. 24, DE-27570 Bremerhaven, Germany
2 Observational Oceanography, Alfred Wegener Institute for Polar and Marine Research, Am Handelshafen 12, DE-27570 Bremerhaven, Germany
3 Norwegian Meteorological Institute, PO Box 43 Blindern, NO-0313 Oslo, Norway
4 Department of Environmental Meteorology, University of Trier, Behringstr. 21, DE-54286 Trier, Germany
5 Spatial Oceanography Laboratory, French Research Institute for Exploration of the Sea, Centre de Brest, FR-29280 Plouzané, France

Correspondence

Polona Rozman, Sea Ice Physics, Alfred Wegener Institute for Polar and Marine and Research, Bussestr. 24, DE-27570 Bremerhaven, Germany.
E-mail: polona.rozman@awi.de

Abstract

A correct representation of the ice movement in an Arctic sea-ice–ocean coupled model is essential for a realistic sea-ice and ocean simulation. The aim of this study is to validate the observational and simulated sea-ice drift for the Laptev Sea Shelf region with in situ measurements from the winter of 2007/08. Several satellite remote-sensing data sets are first compared to mooring measurements and afterwards to the sea-ice drift simulated by the coupled sea-ice–ocean model. The different satellite products have a correlation to the in situ data ranging from 0.56 to 0.86. The correlations of sea-ice direction or individual drift vector components between the in situ data and the observations are high, about 0.8. Similar correlations are achieved by the model simulations. The sea-ice drift speed derived from the model and from some satellite products have only moderate correlations of about 0.6 to the in situ record. The standard errors for the satellite products and model simulations drift components are similar to the errors of the satellite products in the central Arctic and are about 0.03 m/s. The fast-ice parameterization implementation in the model was also successfully tested for its influence on the sea-ice drift. In contrast to the satellite products, the model drift simulations have a full temporal and spatial coverage and results are reliable enough to use as sea-ice drift estimates on the Laptev Sea Shelf.

A faithful simulation of sea-ice velocities in a coupled sea-ice–ocean model is one of the key prerequisites for reliable simulations of sea-ice, ocean and atmosphere parameters. To achieve this, data gathered by manned stations, drifting buoys and lately satellite sensors have been used extensively in pan-Arctic sea-ice model validations (Lemke et al. 1997; Kreyscher et al. 2000; Martin & Gerdes 2007) and data assimilations (Meier et al. 2000; Rollenhagen et al. 2009). For remote coastal regions such as the Laptev Sea Shelf, there are very few ice drift field observations available. Satellite remote-sensing products offer a large improvement in the spatial

and temporal availability of observational data but the retrieval algorithms give products with discontinuous temporal coverage at the grid points closest to the coast (Ezraty et al. 2006; Lavergne et al. 2010) that are consequently hard to inspect for inconsistency.

Sea-ice motion is important in terms of the transport of fresh water and latent heat. Its shear and convergent motion causes dynamical ice growth and influences ice thickness. Sea-ice drift, particularly divergent sea-ice motion, causes leads and polynyas to open. The extensive Laptev Sea polynya system (Fig. 1) is estimated to contribute as much as 20% of the sea-ice area
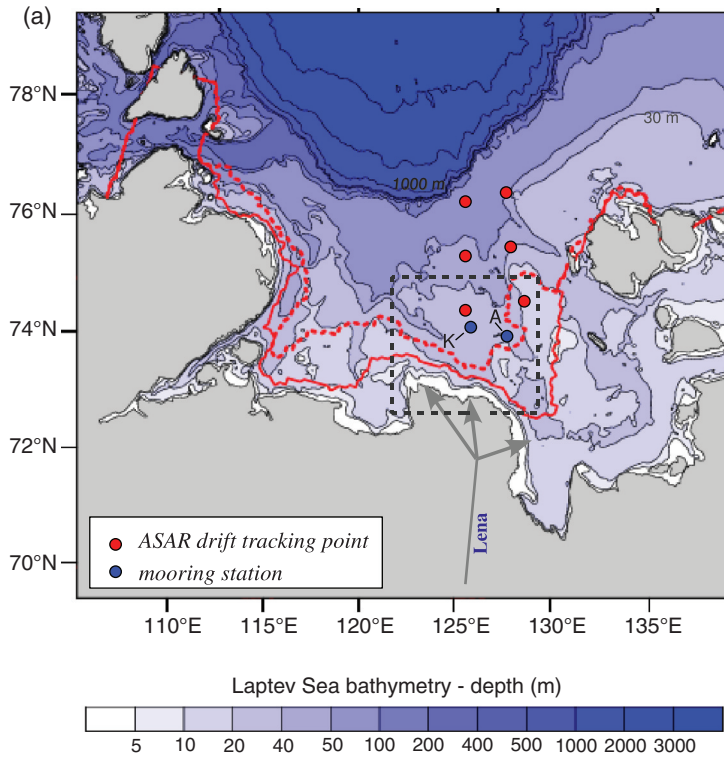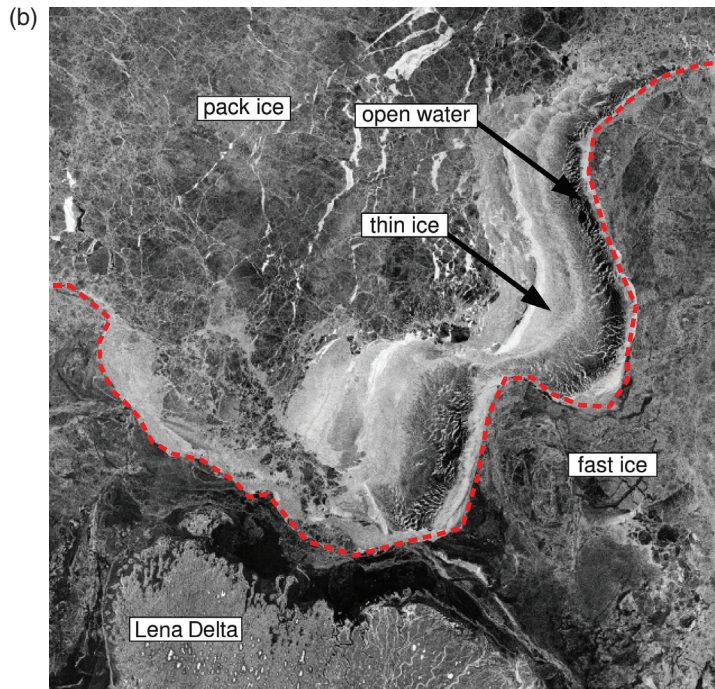
1

Fig. 1 (a) Laptev Sea bathymetry, derived from the *International bathymetric chart of the Arctic Ocean* (Jakobsson et al. 2008). The fast-ice extents in December 2007 (solid red line) and in May 2008 (dashed red line) determine the position of the mid-shelf flaw polynya. Locations of the mooring stations Anabar (A) and Khatanga (K) are shown. The distance from the fast ice edge to the mooring stations changes from about 100 to 20 km, while the distance to the furthermost Advanced Synthetic Aperture Radar (ASAR) tracking point changes from about 300 to 250 km during the winter. The black dashed square represents the area of the ASAR image in (b). (b) ASAR satellite image from 30 April 2008 showing the fast ice in the south-eastern Laptev Sea. The Lena Delta is at the bottom of the image. An advanced flaw polynya with low backscatter values in the open-water area (dark area) developed at the fast-ice edge (dashed red line). The high backscatter values (bright area) in the polynya indicate presence of newly formed ice.

transported through Fram Strait (Rigor & Colony 1997). Despite this there was so far no validation of the sea-ice drift focusing on the Laptev Sea Shelf, where low ice concentrations and fast movements in the polynya zones could influence the quality of the ice drift products (Ezraty et al. 2006).

The North Atlantic–Arctic Ocean–Sea-Ice Model (NAOSIM) that we use in this paper (described in detail further below) gives a relatively good representation of the large-scale Arctic sea-ice features such as the Beaufort Gyre, the Transpolar Drift and sea-ice export out of Fram Strait (Karcher et al. 2003; Martin & Gerdes 2007). However, the performance of this pan-Arctic model for the sea-ice drift over the shelf has not yet been validated. The primary aims of this paper are to examine the quality of the available ice-drift data and use it for a simple validation of the model results on the Laptev Sea Shelf.

Like other sea-ice models, NAOSIM cannot simulate the formation of fast ice (König Beatty & Holland 2010; Adams et al. 2011 [this volume]). Due to this deficiency, the simulated flaw polynya does not occur at the fast-ice edge but directly at the coast instead. The dislocation of the polynya results in severe regional biases in sea-ice concentration, ice growth, ice thickness, winter temperature and salinity distribution. A significantly improved representation of sea-ice concentration as well as ocean temperature and salinity distribution was obtained by including the fast ice in the model (Rozman 2009; Adams et al. 2011). The fast-ice edge region is usually referred to as the mid-shelf, while the regions coastward and seaward from the edge are referred to as the inner shelf and the outer shelf, respectively. The secondary aim of this paper is to show that in the outer shelf the parameterization does not have a significant impact on sea-ice drift.

Data and methods

Observational data

Observational data analysed in this study are in situ data from two moored stations as well as satellite remote-sensing products. Mooring data were retrieved from upward-looking 300 kHz acoustic Doppler current profilers (ADCP; Workhorse Sentinel Teledyne RD Instruments, San Diego, CA, USA) deployed by the Laptev Sea System project in the eastern Laptev Sea mid-shelf. The "Anabar" mooring station was deployed at 74.33°N, 128.00°E at a depth of 30 m and the "Khatanga" mooring station at 74.71°N, 125.29°E at a depth of 43 m (Fig. 1). The devices operated from September 2007 until August 2008, during which time they recorded ice movements at the sea surface above them, as described by Belliveau et al. (1990).

All available sources of satellite-based ice-drift products, regardless of spatial resolution, were used for the validation of the model simulations. Table 1 shows an overview of the data that were used.

The sea-ice drift vectors distributed by the Center for Satellite Exploitation and Research (CERSAT) at the French Research Institute for Exploitation of the Sea (IFREMER) in Plouzané, France, were processed from pairs of Advanced Microwave Scanning Radiometer Earth Observing System (AMSR-E)/Aqua images acquired through 89-GHz channels. The pixel size of the images is 6.25 km (Ezraty et al. 2006). Hereafter we refer to this ice-drift product as "IFREMER". The gridded drift data have a spatial resolution of 31.25 km. For this study, three-day drift vectors were used. The data set is only available from October until the onset of ice melt at the beginning of May and has quality flags indicating the input data and method used for the drift estimation.

Table 1 The overview of the data sets used in the validation.

	Temporal availability	Initial temporal resolution	Source	Spatial resolution	Type	Quality flags	Error estimate
ADCP[a]	Sep 2007–Aug 2008	30 min	Mooring	2 points	E[g]	No	0.0004 m/s[i]
IFREMER[b]	Oct–Apr	3 days	AMSR-E/EOS-Aqua[e]	31.25 km	L[h]	Yes	0.026 m/s, 35°
OSI-SAF[c]	Oct–Apr	2 days	AMSR-E/EOS-Aqua[e]	62.5 km	L[h]	Yes	0.015 m/s
ASAR[d]	Nov–Apr	12 h 4 days	ASAR/Envisat[f]	1° (5 km)	L[h]	No	0.004–0.002 m/s

[a]Upward-looking 300 kHz acoustic Doppler current profilers.
[b]The French Research Institute for Exploitation of the Sea product processed from pairs of Advanced Microwave Scanning Radiometer Earth Observing System/Aqua images.
[c]Observational data from the European Organization for the Exploitation of Meteorological Satellites Ocean and Sea Ice Satellite Application Facility.
[d]Advanced Synthetic Aperture Radar images.
[e]Images from the Advanced Microwave Scanning Radiometer aboard the Earth Observing System/Aqua satellite.
[f]Images from the Advanced Synthetic Aperture Radar aboard the Envisat satellite.
[g]Eulerian motion.
[h]Lagrangian motion.
[i]The error estimate for the acoustic Doppler current profiler given here is a mean error velocity of the Khatanga mooring record. This error is estimated on the basis of the difference between the velocities measured by the four beams of the device and is a measure combining horizontal homogeneity and errors caused by malfunctioning equipment (Gordon 1996). The error for the Anabar mooring, which was later corrected for the compass bias, is larger: 0.001 m/s.

The second ice-drift product used for the validation is the low-resolution sea-ice drift data set (62.5 km equally spaced grid) of the European Organization for the Exploitation of Meteorological Satellites Ocean and Sea Ice Satellite Application Facility (OSI-SAF; Lavergne et al. 2010) also processed from AMSR-E images and available from October to May. In contrast to the IFREMER product, it computes two-day ice motion vectors from 37-GHz channels (12.5 km pixel size), hence the coarser spatial resolution. The Laptev Sea has many coastal areas and two vast archipelagos. Consequently, the coarse resolution of the latter product considerably limits its use for comparison in the southernmost parts of the sea. No OSI-SAF data are available at the Khatanga mooring location so a point located north of the station was analysed instead.

The third ice-drift product we generated from Advanced Synthetic Aperture Radar (ASAR) satellite images. An ASAR image covers an area of approximately 400×800 km^2 with a spatial resolution of 150×150 km^2 (Cordey et al. 2004). We used the ASAR scenes for the sea-ice drift detection at the mooring locations and at six locations in the eastern Laptev Sea outer shelf (Fig. 1) chosen in a way to form a 1° grid. We manually tracked the movements of distinct ice floes in the vicinity of these points to obtain drift vectors. The floes were tracked inside a search window with a radius proportional to the scale of the ice drift. Floes that drifted directly through the grid points were preferentially selected. On average the search window radius was less than 5 km. The ASAR images were available from November until April with major gaps in January and March. The time difference between two images varies from two to four days.

The estimated errors of the satellite remote-sensing data are low. Validation of both the IFREMER three-day ice drift and the OSI-SAF two-day product have been conducted against drifting buoys in the central Arctic (Ezraty et al. 2006; Lavergne et al. 2010). For the IFREMER product, Girard-Ardhuin & Ezraty (2005) report standard deviations of 6.7 km and 35° that corresponds to 0.026 m/s uncertainty for the drift speed. For the OSI-SAF product, Lavergne et al. (2010) document a standard deviation of 2.6 km that translates into 0.015 m/s uncertainty for the zonal and meridional drift component. One should note, however, that the reference data sets used for both validation exercises were different, as were the collocation methods and time period.

The ASAR drift was extracted from the geolocated images. The geolocation uncertainty could result in an error of up to two pixels (300 m; Rosich & Meadows 2004). We estimate that the deformation of the tracked

ice floe could contribute to an error of another one to three pixels and therefore result in a drift error for the tracked floe of around 0.004 m/s. The true error of the ASAR drift compared to the real velocities at the tracking points (position of the tracked ice floe was not exactly at the tracking point) is unknown. The ice-drift situation in the four northern points was homogeneous, while the southernmost points were very close to the flaw polynya where the sea-ice drift is more heterogeneous.

Model description

The NAOSIM is a coupled sea-ice–ocean model developed at Alfred Wegener Institute for Polar and Marine Research (Gerdes et al. 2003; Karcher et al. 2003; Fieg et al. 2010). The model domain encloses the northern North Atlantic, the Nordic seas and the Arctic Ocean. The highest resolving version of NAOSIM (Fine Resolution Model) has a horizontal grid spacing of 1/12° on a rotated spherical grid where the Equator runs across the North Pole. Near the surface vertical resolution is 10 m. The ocean component of the model is based on the Modular Ocean Model MOM-2 of the Geophysical Fluid Dynamics Laboratory (Pacanowski 1995). It is coupled to a dynamic–thermodynamic sea-ice model (Hibler 1979) that employs a viscous-plastic rheology. The wind forcing in this experiment was taken from the six-hourly US National Centers for Environmental Prediction/National Center for Atmospheric Research (NCAR/NCEP) reanalysis data. Fast-ice information (Fig. 1a) was integrated in the model in such a way that the fast-ice covered cells were excluded from the calculation of the sea-ice momentum balance. Fast ice remained at rest while all thermodynamic calculations were performed as usual. Such a procedure has been successfully applied by Lieser (2004), who used a fast-ice parameterization on the basis of sea-ice thickness and bathymetry in a 1/4° model. To enable a realistic representation of the flaw polynya processes in our high-resolution model, we used prescribed high-resolution fast-ice area instead. Monthly fast-ice masks for winter 2007/08 (from December to May) were obtained from thermal bands of the Moderate Resolution Imaging Spectroradiometer (MODIS) sensor aboard the Earth Observing System (EOS)/Aqua satellite (Adams et al. 2011).

Data analysis methods

All ice drift data, modelled and observed, were converted to three-day running means of ice drift to average out tidal and inertial movements of sea ice and obtain comparable quantities. The OSI-SAF two-day means

were first divided into daily means and then re-averaged to three-day means. The low temporal resolution did not allow a complete averaging of the ASAR drift estimates for which, in some cases, single values were used to represent the three-day period. The satellites carrying AMSR-E and ASAR sensors fly over the Laptev Sea twice per day, usually at noon and midnight. The three-day means in all of the AMSR-E products are calculated from noon on the first day until noon on the fourth day (in total three to a maximum of eight overflights as the neighbouring scenes overlap at high latitudes). To avoid a phase shift between the data sets also the mooring and modelled ice drift was calculated for the same time window. As noon images of ASAR are rare, most of the images we analysed were taken at midnight (typically 02:00–0:300 UTC) and consequently the ASAR time series still have a small time shift compared to other time series.

We converted the data on the meridional and zonal sea-ice movement to two sea-ice drift properties—speed (magnitude) and direction (angle)—and analysed them separately. We first examined the time series of speed and sine of direction for all data sets and checked that there is no or minimal time shift between them. Below we present the results of the linear regression analysis for the correlations between the observational data sets for speed and circular regression for the directional correlations.

The ADCP record has the full time coverage and is the only data set measured in situ at the drifting ice surface. Despite this the mooring record represents a point measurement, while the satellite products represent gridded information (like the model output) produced from individual daily snapshots. No mooring with an ice drift recording device has ever been recovered in the Laptev Sea outer shelf. In this paper we therefore compared the ADCP data to all other observational data sets in the mid-shelf. In the outer shelf, where no such data are available, we made a cross-comparison of all other data. Below we show the correlations between the observational data and the model simulations. We also analysed the observational data—if available—with the best quality flags only. We compare, below, the zonal and meridional drift vectors of all satellite remote-sensing products and model simulations to the in situ data. This eases the comparison with previously published validation statistics for the central Arctic.

Statistics such as linear regression analysis are not appropriate for the analysis of the circular data where the numerical value for the parameter depends on the assignment of zero-direction and direction of rotation. The angles such as 0° and 359° are as numerical values

very distant and would result in erroneous mean values if regular arithmetic mean is applied. Various circular (directional) statistics methods have been suggested and used over the past decades to overcome this problem (Fisher 1996; Jammalamadaka & Sengupta 2001). The mean of an angular data set is computed by treating all angular measurements as points on a unit circle and computing the resultant vector of the unit vectors determined by the data points (Fisher 1996; Jammalamadaka & Sengupta 2001). The mean direction is the direction of this resultant vector and the mean resultant length provides a measure of concentration of the circular data. For the angular data a with statistical population n, mean direction $\bar{\alpha}$ is defined as

$$
\bar{\alpha} = \begin{cases} \arctan\left(\dfrac{S}{C}\right) & \text{if } S > 0, C > 0 \\[2mm] \arctan\left(\dfrac{S}{C}\right) + \pi & \text{if } C < 0 \\[2mm] \arctan\left(\dfrac{S}{C}\right) + 2\pi & \text{if } S < 0, C > 0, \end{cases}
$$

where S and C are

$$
S = \sum_{i=0}^{n} \sin(\alpha_i)
$$

$$
C = \sum_{i=0}^{n} \cos(\alpha_i)
$$

The circular variance is defined as $1 - \bar{R}$ where $R = \sqrt{S^2 + C^2}$ and $\bar{R} = R/n$. Its values fall in the interval [0, 1], where data highly concentrated around one direction take values close to 0, while widely dispersed data have values close to 1. Statistical mean and variance for linear variables x, y or circular variables α, β were then used for calculation of statistical bias ($\bar{x} - \bar{y}$ or $\bar{\alpha} - \bar{\beta}$) and variance ratio $F(var_x/var_y$ or $var_\alpha/var_\beta)$

One of the possible measures of correlations between two circular variables was suggested by Jammalamadaka & Sengupta (2001), who defined the circular correlation coefficient $r_{\alpha\beta}$ for two angular data sets α and β as:

$$
r_{\alpha\beta} = \frac{\sum_{i=1}^{n} \sin(\alpha_i - \bar{\alpha})\sin(\beta_i - \bar{\beta})}{\sqrt{\sum_{i=1}^{n} \sin^2(\alpha_i - \bar{\alpha}) \sin^2(\beta_i - \bar{\beta})}}.
$$

If α and β are independent, $r_{\alpha\beta}$ is close to 0 and if the two variables are rotationally dependent $r_{\alpha\beta}$ would be close to ± 1. The correlation is then defined as $r_{\alpha\beta}^2$. This is an analogue formula to the classical linear regression correlation coefficient in which for two linear variables x and y the correlation coefficient r_{xy} is defined as:

$$r_{xy} = \sum_{i=1}^{n} \frac{(x_i - \bar{x})(y_i - \bar{y})}{\sigma_x \sigma_y}.$$

Results

Observed sea-ice drift

Figure 2 shows scatter diagrams and statistical coefficients for the Khatanga and Anabar mooring locations in the mid-shelf. The ADCP and IFREMER data sets agree well in the direction of the drift. The statistical correlation between data sets are high ($r^2 = 0.8$), statistical bias is low and variance ratio (F) is close to 1. The correlations of ASAR and OSI-SAF data sets to the ADCP record are lower ($r^2 = 0.6$) with both ASAR and OSI-SAF data sets underestimating the ADCP measured speeds. There was no OSI-SAF drift point available for the exact Khatanga location and a point further off-shore was analysed instead. Consequently, it is not surprising that the correlations of all data sets with the OSI-SAF are moderate.

On the outer shelf correlations between the data sets are higher than in the mid-shelf region (r^2 from 0.65 to over 0.8). In Fig. 3 we show scatter diagrams and statistical coefficients for the combination of data for all six points on the ASAR grid.

Simulated sea-ice drift

When compared to the observed ice drift, the time series in Figs. 4 and 5 show that the model simulates the sea-ice drift speed and direction well. The model is underestimating the ADCP velocities but is simulating all of the peak speed events from the consolidation of the sea-ice cover in November and onwards. The directions during the high speed events are represented correctly. Erroneous drift directions occur mainly during the events with low drift speed. The speeds lower than 0.035 m/s would contribute to a displacement up to 9 km during the three-day averaging period. As this movement is a subgrid process for a model with 1/12° horizontal grid resolution, we excluded this directions from the circular regression analysis. The displacements smaller than half of a pixel (3.12 km for IFREMER product and 6.25 km for OSI-SAF) are also not detectable by the tracking algorithms. Apart from a slight reduction in speed in the second part of the winter there is no significant change in ice drift simulation after the integration of the fast ice for any of the analysed locations on the mid- or outer shelf (Figs. 4, 5).

Figures 6 and 7 show scatter diagrams and statistical coefficients of the observational data and the model simulations. The model speed simulations have low

statistical bias compared to all observational data but the variance ratio (F) is high when compared to all of the data sets, except compared to the ASAR drift speed. The simulated directions have a moderate bias but a variance ratio (F) slightly lower than 1.

The simulated sea-ice speed at the mooring locations and in the outer shelf is moderately correlated to the observational speeds (r^2 from 0.4 to 0.7). The regression line shows a general underestimation of the speed compared to observations. Once the directions simulated at low speeds were removed from the statistical analysis the circular correlations to the observational data sets are moderate to high (r^2 from 0.5 to 0.9). Using only the best quality flags for the IFREMER and OSI-SAF data sets reduces the number of data points in time but the correlations do not improve.

Drift vector validation

The comparison of the zonal and meridional drift component of satellite products and model simulations to the in situ data shows high correlations (r^2 higher than 0.7; Table 2) but higher standard deviations of errors as in the central Arctic Basin (Table 1). The mean measured error velocity for the Khatanga mooring ADCP is 0.0004 m/s (Table 1), while the error velocity for the Anabar, which compass bias was calibrated only after the instrument was recovered, is 0.001 m/s. For the model again only the drifts with speed higher than 0.035 m/s were analysed.

Discussion

The observational data and model simulations were compared at two mooring locations in the mid-shelf dominated by the polynya activity and at six regularly spaced points in the outer shelf region where the thin ice gradually grows into the pack ice.

The comparison of the satellite observational data shows that ice drift directions are all moderately to highly correlated to the ADCP record. The IFREMER product is also highly correlated in speed. The ASAR and OSI-SAF speeds are only moderately correlated but given the temporal and spatial mismatch this is a relatively good result. While the ASAR data sets still have a small phase shift due to prevailing midnight overflights and three-day averages based on a small number of images, the OSI-SAF product does not cover the Khatanga mooring location and an alternative location further offshore was used in comparison.

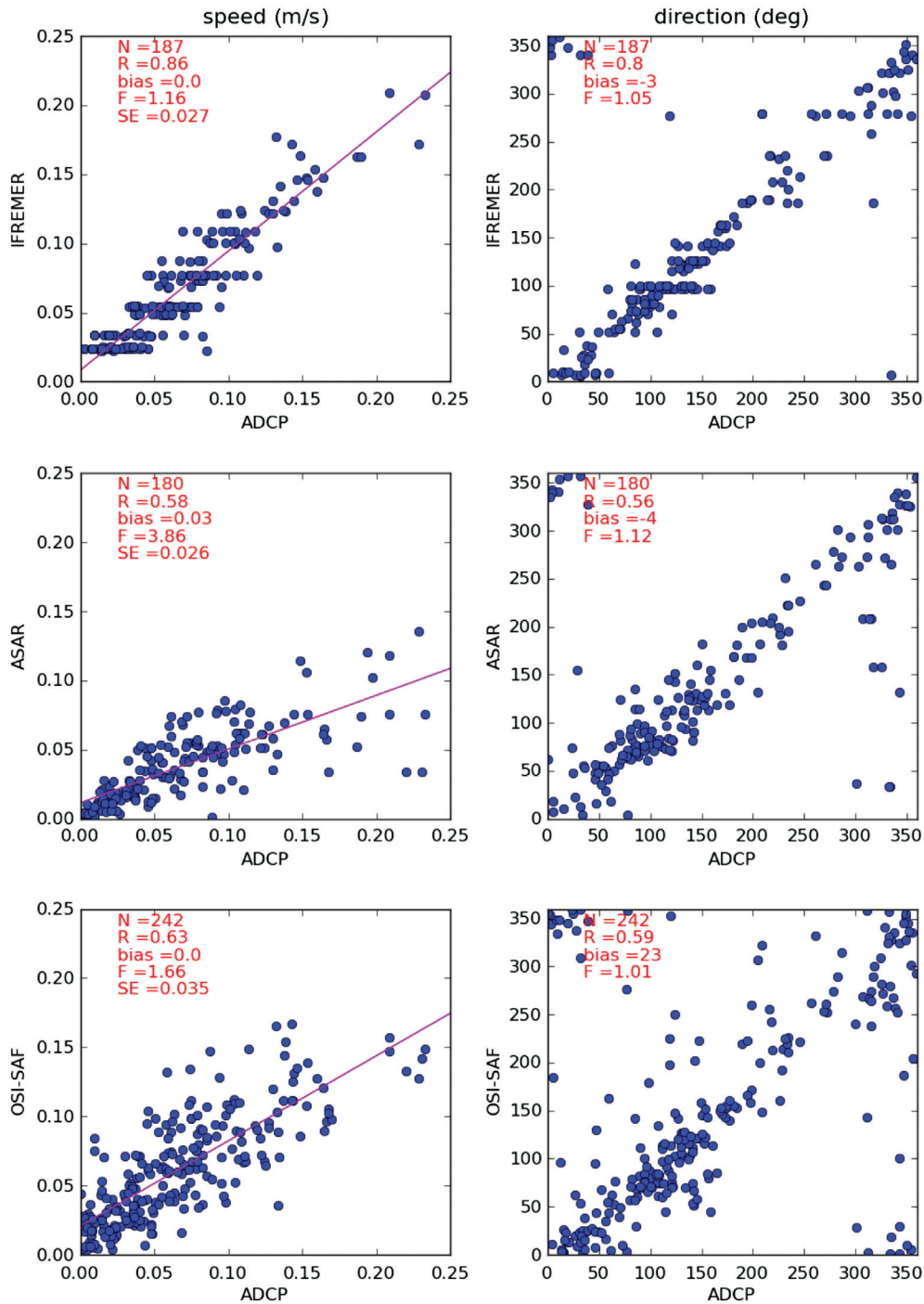The scatter diagrams in Figs. 2 and 3 show that the IFREMER data set only occupies certain discrete values.

Fig. 2 Scatter plots of sea-ice drift speed and direction at the Anabar and Khatanga mooring locations for the period from November 2007 to May 2008 derived from upward-looking 300 kHz acoustic Doppler current profilers (ADCP) compared to the following data sets: Advanced Synthetic Aperture Radar (ASAR) images, the French Research Institute for Exploitation of the Sea product (IFREMER) processed from pairs of Advanced Microwave Scanning Radiometer Earth Observing System/Aqua images and observational data from the European Organization for the Exploitation of Meteorological Satellites Ocean and Sea Ice Satellite Application Facility (OSI-SAF). Each plot shows the number of data pairs in the analysis (*N*), the correlation value (*R*), the statistical bias (bias), the variance ratio (*F*) and the standard error deviation (SE). Speed units are m/s and direction values are degrees. All correlations shown are statistically significant at the 99% confidence level (probability value less than 0.001).
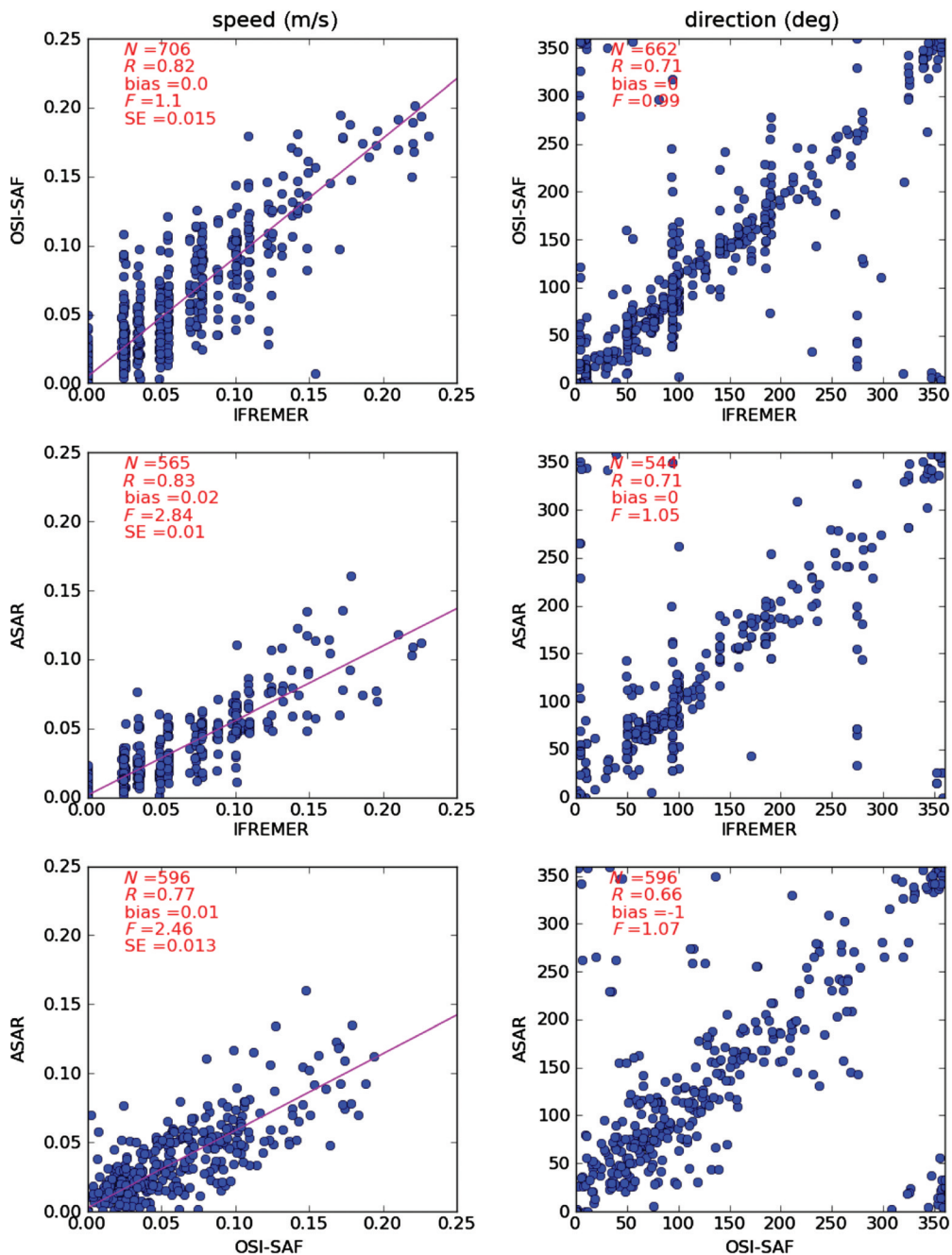
Fig. 3 Scatter plots of sea-ice drift speed and direction in the outer shelf for the period from November 2007 to May 2008 using the following data sets: Advanced Synthetic Aperture Radar (ASAR) images, the French Research Institute for Exploitation of the Sea product (IFREMER) processed from pairs of Advanced Microwave Scanning Radiometer Earth Observing System/Aqua images and observational data from the European Organization for the Exploitation of Meteorological Satellites Ocean and Sea Ice Satellite Application Facility (OSI-SAF). Each plot shows the number of data pairs in the analysis (*N*), the correlation value (*R*), the statistical bias (bias), the variance ratio (*F*) and the standard error deviation (SE). Speed units are m/s and direction values are degrees. All correlations shown are statistically significant at the 99% confidence level (probability value less than 0.001).

This "quantization noise" is a well-known effect of the robust Maximum Cross Correlation method (Kwok et al. 1998; Girard-Ardhuin & Ezraty 2005; Lavergne et al. 2010) that the IFREMER data set algorithm uses for the ice drift estimation. The effect causes no obvious problems at this stage of the model validation. The OSI-SAF product uses the Continuous Cross Correlation Method (Lavergne et al. 2010), which avoids this problem.
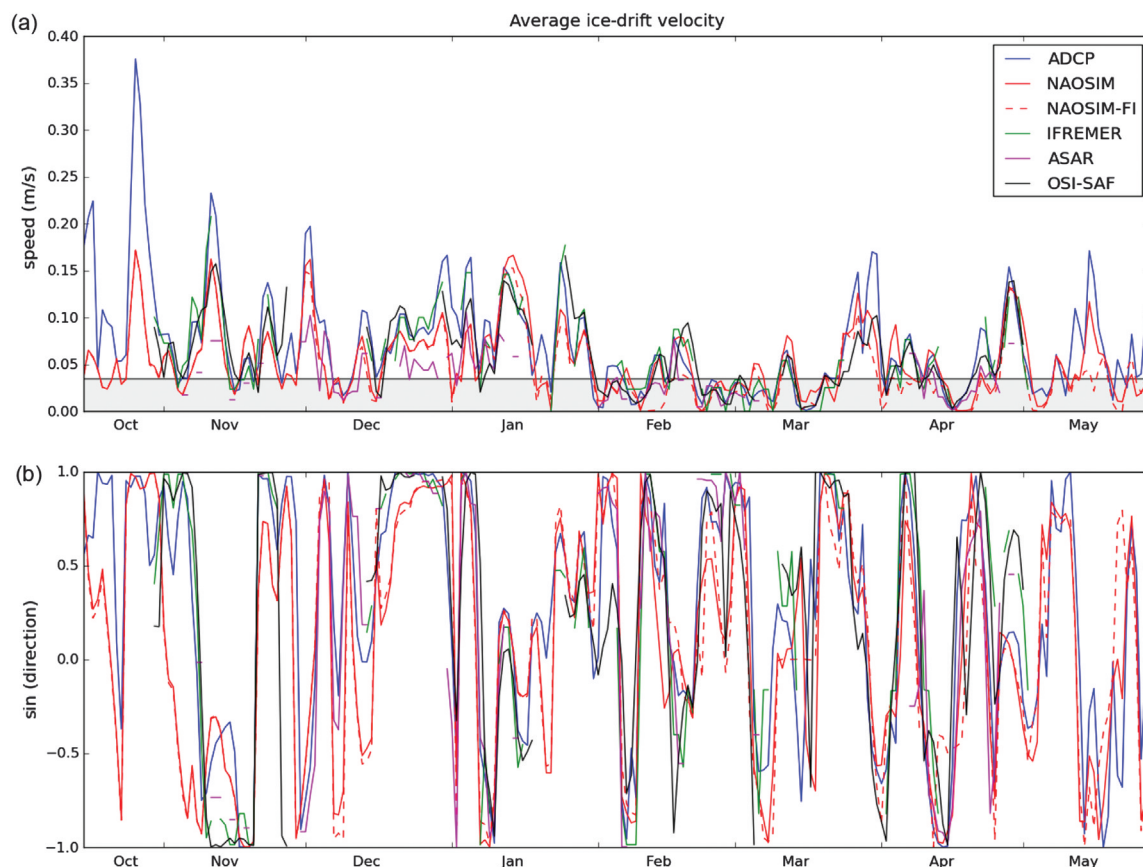
Fig. 4 (a) Sea-ice drift speed and (b) direction without (red line) and with (dashed red line) integrated fast ice derived from two versions of the North Atlantic–Arctic Ocean–Sea-Ice Model (NAOSIM and NAOSIM-FI) and the following observational and remote-sensing data sets for the Khatanga mooring location from 15 October 2007 to 15 May 2008: upward-looking 300 kHz acoustic Doppler current profilers (ADCP), Advanced Synthetic Aperture Radar (ASAR) images, the French Research Institute for Exploitation of the Sea product (IFREMER) processed from pairs of Advanced Microwave Scanning Radiometer Earth Observing System/Aqua images and observational data from the European Organization for the Exploitation of Meteorological Satellites Ocean and Sea Ice Satellite Application Facility (OSI-SAF). The grey-filled rectangle in (a) marks speeds that were not included in the directional correlation analysis.

For the mooring locations the model simulation is in good agreement with the ADCP and satellite remote-sensing data (Fig. 4). The simulated ice drift speeds compared to these data sets are very similar starting from November, when the sea-ice cover in the Laptev Sea becomes relatively stable. It is remarkable that the simulated and ADCP speeds match not only in phase but also in magnitude and the model is able to simulate the early winter extreme velocities (peaks in Fig. 4). The ice drift directions are similar for the whole observation period. They match especially well during the high speeds. The time series also show the scarcity of the satellite retrieved data, which may have gaps weeks in length.

The statistical bias of the model results is much lower on the outer shelf than on the mid-shelf. The variance ratio (F) of directions decreases on the outer shelf as well and shows that the simulated model directions are more dispersed than the observed directions.

The correlations between all of the observational data and the model simulations are slightly higher on the mid-shelf than on the outer shelf. This is surprising since in the dynamic mid-shelf environment, dominated by polynya events, the model should have more difficulties with correct simulations than on the relatively homo-geneous outer shelf. The reason for this unexpected result is probably a smaller number of observations analysed on the mid-shelf. Because we decided to exclude all of the drift directions for drift speed lower than 0.035 m/s, a relatively larger part of the data was excluded on the mid-shelf, where the ice velocity is generally lower and only the fastest movements (top
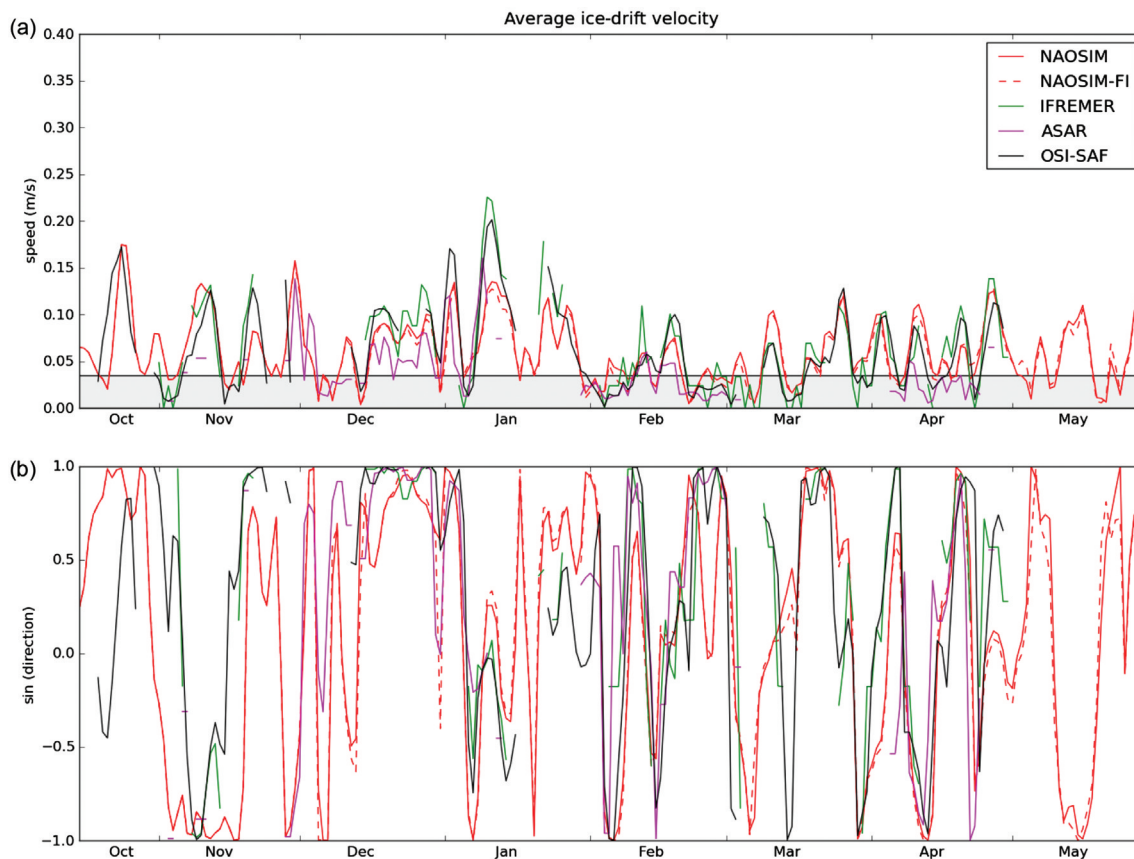
Fig. 5 (a) Sea-ice drift speed and (b) direction without (red line) and with (dashed red line) integrated fast ice derived from two versions of the North Atlantic–Arctic Ocean–Sea-Ice Model (NAOSIM and NAOSIM-FI) and the following observational and remote-sensing data sets for a point on the outer shelf (77°N, 125°E) from 15 October 2007 to 15 May 2008: Advanced Synthetic Aperture Radar (ASAR) images, the French Research Institute for Exploitation of the Sea product (IFREMER) processed from pairs of Advanced Microwave Scanning Radiometer Earth Observing System/Aqua images, and observational data from the European Organization for the Exploitation of Meteorological Satellites Ocean and Sea Ice Satellite Application Facility (OSI-SAF). The grey-filled rectangle in (a) marks speeds that were not included in the directional correlation analysis.

50%) of the data entered the analysis. In the outer shelf almost 70% of all data entered the analysis.

There is still some remaining phase shift (Fig. 4) between the model and the observations due to the temporal resolution of the wind forcing data. The six-hour wind situation does not represent the wind changes during the six-hour interval. The time shift error is occurring randomly and depends on the timing of the wind direction change. This error can only be excluded by a high enough temporal resolution of the forcing data or by full coupling of the model.

Furthermore, differences in observed drift also arise because the measurement techniques are principally different. The model and the mooring velocities are Eulerian while the remote sensing velocities are Lagrangian. The high correlation between the ADCP and the IFREMER data shows that the averaged Lagrangian

velocities around the mooring location are comparable to the Eulerian velocities measured over the mooring station. The classical sea-ice drift validation was done with the drifting buoys that also represent a Lagrangian type of measurement (Ezraty et al. 2006; Lavergne et al. 2010). The IFREMER and OSI-SAF drift products are spatial averages, while the ADCP record and ASAR drift data represent a non-averaged single point/floe drift. Each drift vector from the OSI-SAF product pertains to an area of approximately 120×120 km^2 while the IFREMER vectors pertain to roughly 60×60 km^2 (four times less), thanks to the higher resolution of the 89-GHz channels. These results were then gridded to the spatial resolutions of 62.5 km and 31.25 km, respectively.

The model simulations and the ASAR data set systematically underestimate the in situ measured speed, when velocities are higher than 0.1 m/s. The reasons for too

low simulated drift speeds could be found in a too low wind stress or a high ocean drag influencing the momentum balance of the sea-ice in the model. The ASAR data set peak speeds are systematically lower than the ones of IFREMER, OSI-SAF and ADCP by about a half. For the ASAR drift only remarkable features in sea-ice, such as big pressure ridges and hummocks, were used for tracking. Despite a great surface roughness, detectable also by high backscatter signatures on the ASAR images, these features do not drift as fast as one would expect from a greater wind stress acting on their sails. It seems that the friction between rough jagged floes is an important sink of energy for shearing at floe boundaries (Rothrock 1975). The big ice floes, as used for tracking on the ASAR images, are therefore less appropriate for the estimation of the prevailing ice drift situation. The ASAR velocities that have been retrieved specifically for this research have still been proven to be a useful alternative source of information, independent from other satellite remote-sensing products. In November and December, when there are occasionally no AMSR-E ice drift products available (Figs. 4, 5), ASAR derived speed and direction are similar to the in situ measured speed and direction and to the simulated speed and direction.

The standard deviations of the error for the satellite products and model simulations validated with the ADCP record are about 0.03 m/s (Table 2). Compared to the buoy validation performed in the central Arctic and Canadian Arctic Archipelago these errors are slightly higher (for 0.005 m/s) for the IFREMER (Ezraty et al. 2006) and double for the OSI-SAF product (Lavergne et al. 2010). This confirms our hypothesis that the errors of the estimates are higher over the shelf seas. The in situ ice drift velocities measured in the Laptev Sea mid-shelf are relatively higher than in the buoy validation set that was used by Ezraty et al. (2006) and Lavergne et al. (2010). A part of this error can certainly be attributed to the inhomogeneous drift environment in the mid-shelf. The data sets used in this paper also exhibit frequent peaks in speeds over 0.1 m/s, while such events in the buoy data sets were not common. This suggests that despite the larger errors the satellite and simulated velocities are still relatively good estimates.

The fast-ice parameterization has no major impact on the ice drift simulations apart from additionally reducing the drift speed in the mid-shelf region during the periods with low speeds (in our case, from February on). This effect is hardly detectable further offshore (Fig. 5). The correlations of model results with and without fast-ice parameterization with the observational data are similar (Figs. 6, 7).

The NAOSIM was already validated by Martin and Gerdes (2007) with the product merged from Quick Scatterometer and Special Sensor Microwave/Imager drift estimations provided by CERSAT/IFREMER. The product has a spatial resolution of 62.5 km and is available for the central Arctic only. Using monthly means from three- or six-day products the validation was performed for the period 1992–2001. The NAOSIM, similarly to other models in the Arctic Ocean Model Intercomparison Project, slightly overestimated the drift speeds. The model also had a slight deviation of the drift angles to the right. On the other hand, on the Laptev shelf NAOSIM underestimates the drift speed and has a slight angle deviation to the left. This again points at the systematic differences between the central Arctic and the shelf seas.

The Arctic Ocean Model Intercomparison Project revealed differences between the simulations of different coupled sea-ice–ocean models. Although it has been estimated that 70% of the short-term ice drift variability is explained by wind variability (Thorndike & Colony 1982) and the models in the project all used identical atmospheric forcing, the resulting sea-ice drift simulations differed substantially (Martin & Gerdes 2007). To explain the differences in the model performances, Martin & Gerdes pointed out the differences in the implementation of the atmospheric and oceanic forcing, among them the actual prescription of the wind stress and the implementation of the ocean–ice drag term.

In this case study, the correlation of sea-ice drift simulated by NAOSIM to the in situ data in sea-ice direction or individual vector components largely exceeds 70% of the variability that should be explained by the wind variability (Thorndike & Colony 1982). This means that not only wind stress but also other important contributors to the sea-ice momentum balance, such as the ocean–ice drag, the internal sea-ice stress and the Coriolis force (Harder et al. 1998), are realistically implemented in the model. Another evidence for the role of the ocean and ice dynamics in the model is the spatial variability between the drift records at the Khatanga mooring location (Fig. 4) and in the outer shelf (Fig. 5). The difference between the two time series is much larger than expected from a difference between two grid points of the wind forcing data with a spatial resolution of 1.875° (Kanamitsu et al. 2002).

Conclusions

In this paper we used unique in situ sea-ice drift records from the Laptev Sea shelf to validate satellite remote-sensing products and model simulations. Our results show the following. (1) The fast-ice parameterization in
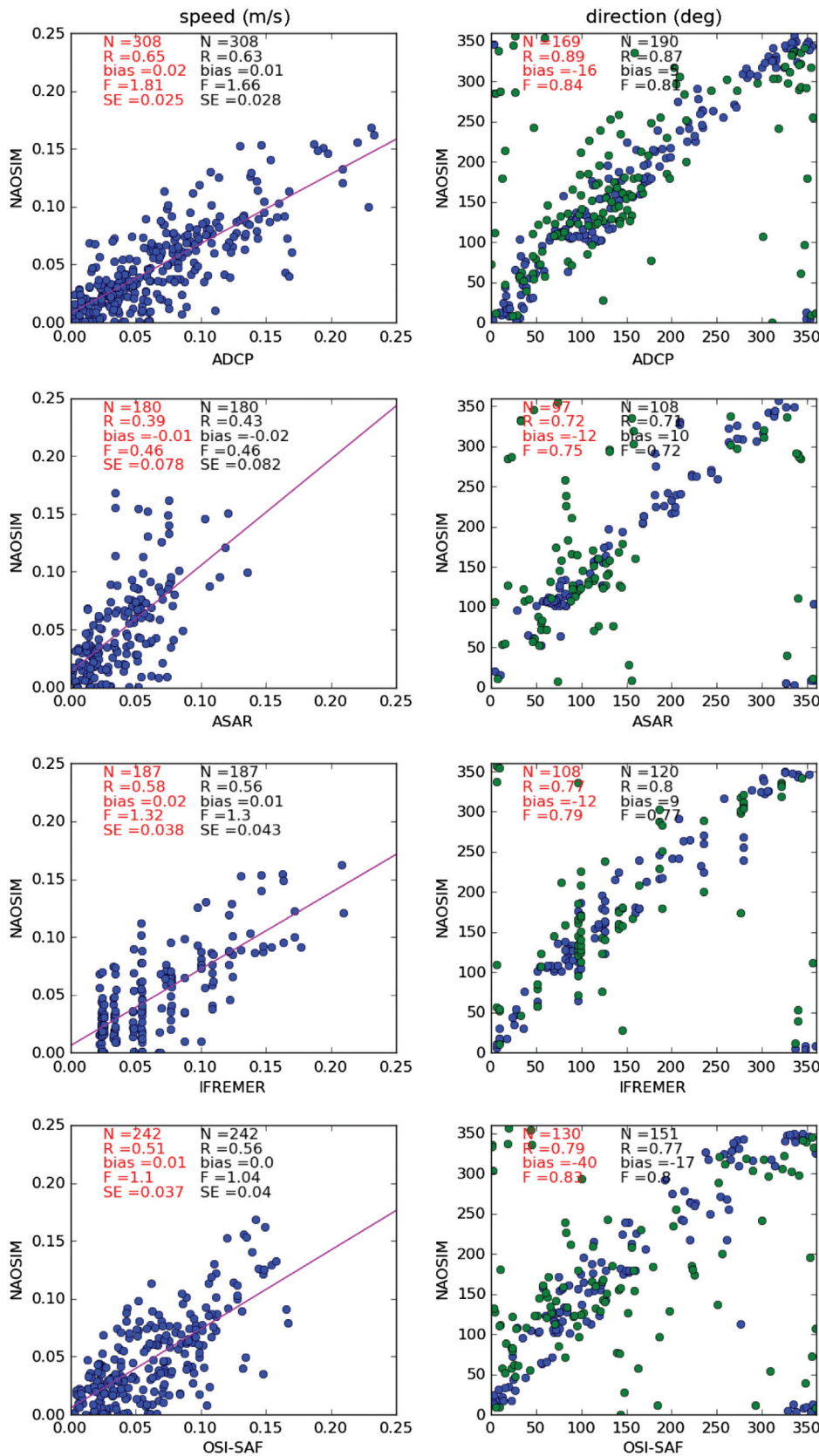
Fig. 6 Scatter plots of sea-ice drift speed and direction at the Anabar and Khatanga mooring locations as simulated with the fast ice by the North Atlantic–Arctic Ocean–Sea-Ice Model (NAOSIM) for the period from November 2007 to May 2008 compared to the following data sets: upward-looking 300 kHz acoustic Doppler current profilers (ADCP), Advanced Synthetic Aperture Radar (ASAR) images, the French Research Institute for Exploitation of the Sea product (IFREMER) processed from pairs of Advanced Microwave Scanning Radiometer Earth Observing System/Aqua images and observational data from the European Organization for the Exploitation of Meteorological Satellites Ocean and Sea Ice Satellite Application Facility (OSI-SAF). Blue dots are data points included in the statistical analysis. The points with drift speed under 0.035 m/s at the drift direction scatter plots are marked by green dots. Each plot shows the number of data pairs in the analysis (*N*), the correlation value (*R*), the statistical bias (bias), the variance ratio (*F*) and the standard error deviation (SE). Speed units are m/s and direction values are degrees. All correlations shown are statistically significant at the 99% confidence level (probability value less than 0.001). Numbers in red (black) show the statistical characteristics of the model simulations with (without) the fast ice.
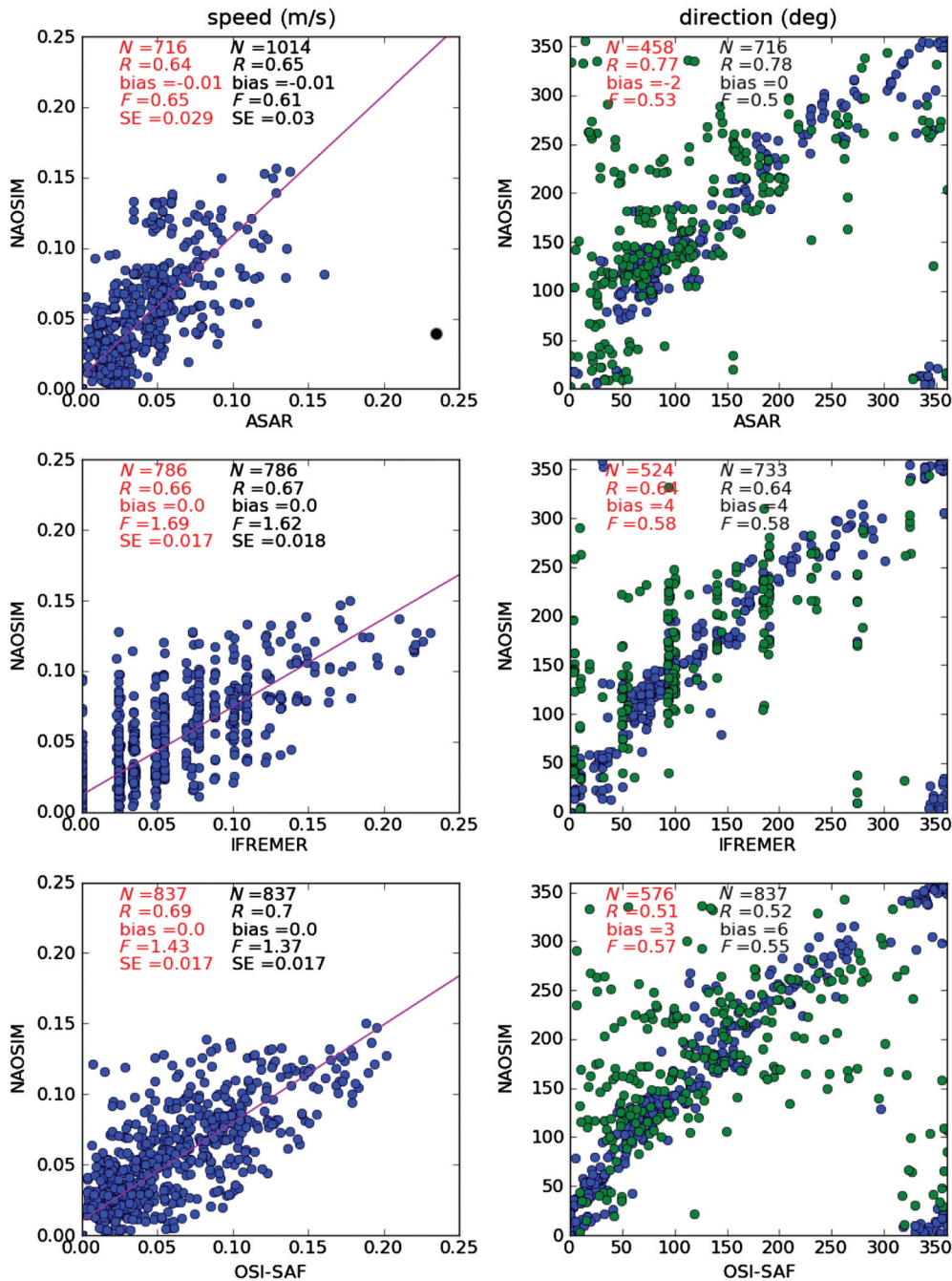
Fig. 7 Scatter plots of sea-ice drift speed and direction at in the outer shelf as simulated by the North Atlantic–Arctic Ocean–Sea-Ice Model (NAOSIM) for the period from November 2007 to May 2008 compared to the following data sets: Advanced Synthetic Aperture Radar (ASAR) images, the French Research Institute for Exploitation of the Sea product (IFREMER) processed from pairs of Advanced Microwave Scanning Radiometer Earth Observing System/Aqua images, and observational data from the European Organization for the Exploitation of Meteorological Satellites Ocean and Sea Ice Satellite Application Facility (OSI-SAF). Model simulation with the fast ice and observational data comparison from November 2007 to May 2008. Blue dots are data points included in the statistical analysis. Green dots are points with drift speed under 0.035 m/s. Each plot shows the number of data pairs in the analysis (N), the correlation value (R), the statistical bias (bias), the variance ratio (F) and the standard error deviation (SE). Speed units are m/s and direction values are degrees. All correlations shown are statistically significant at the 99% confidence level (probability value less than 0.001). Numbers in red (black) show the statistical characteristics of the model simulations with (without) the fast ice.

Table 2 The validation results of the drift vector components of the satellite products and model simulations with the in situ measurements for the Laptev Sea mid-shelf in winter 2007/2008.

	N	$Bias_{\vec{u}}$	$Bias_{\vec{v}}$	$SD_{\vec{u}}$	$SD_{\vec{v}}$	$r_{\vec{u}}^2$	$r_{\vec{v}}^2$
IFREMER[a]	187	−0.006	0.002	0.030	0.027	0.90	0.93
OSI-SAF[b]	242	0.040	0.006	0.040	0.031	0.69	0.84
ASAR[c]	180	0.003	0.005	0.027	0.021	0.73	0.86
NAOSIM[d]	190	0.005	0.014	0.033	0.025	0.85	0.87
NAOSIM-FI[d]	169	0.009	0.014	0.037	0.025	0.84	0.87

Note: The columns show statistical parameters for the zonal $\vec{u}$ and meridional $\vec{v}$ components of the drift: number of data pairs in the analysis (N), statistical bias (bias), standard error deviation (SE) and correlation value (r^2). Velocity units are m/s. All correlations shown are statistically significant at the 99% confidence level (probability less than 0.001).
[a]The French Research Institute for Exploitation of the Sea product processed from pairs of Advanced Microwave Scanning Radiometer Earth Observing System/Aqua images.
[b]Observational data from the European Organization for the Exploitation of Meteorological Satellites Ocean and Sea Ice Satellite Application Facility.
[c]Advanced Synthetic Aperture Radar images.
[d]Two versions of the North Atlantic–Arctic Ocean–Sea-Ice Model.

the model has no major impact on the sea-ice drift simulations and its smoothing effect disappears at distances larger than 100 km (about 10 model grid points). (2) The standard deviations of the error for the satellite products validated with the in situ record are larger on the shelf than in the central Arctic. The errors for the satellite products and model simulations are about 0.03 m/s. (3) The sea-ice drift remote-sensing products give better estimates than the in situ mooring records for the shelf regions. The high-resolution IFREMER product has an especially strong correlation and low standard deviation compared to the in situ data. (4) For the validation of the sea-ice drift on the Eurasian shelf simulated by the eddy-resolving sea-ice models, we recommend the use of the in situ data and high-resolution satellite retrieved products. Because of the differences between the products in our validation we recommend using more than one satellite product for the validation. (5) The correlation of simulated sea-ice drift to the in situ data in sea ice direction or in individual vector components is at least 0.84. To achieve a more realistic simulations of the drift speed, the calculation of the wind stress and ocean drag terms should be studied closely. The model drift simulation have, contrary to the satellite products, a full temporal and spatial coverage and the correlations to the in situ data are high enough to use them as sea-ice drift estimates on the Laptev Sea Shelf.

Acknowledgements

References

Adams S., Willmes S., Heinemann G., Rozman P., Timmermann R. & Schröder D. 2011. Evaluation of simulated sea-ice concentrations from sea-ice/ocean models using satellite data and polynya classification methods. *Polar*

Research 30, article no. 7124, doi: 10.3402/polar.v30i0.7124 (this volume).

Belliveau D., Bugden G., Eid B. & Calnan C. 1990. Sea ice velocity measurements by upward-looking Doppler current profilers. *Journal of Atmospheric and Oceanic Technology 7,* 596–602.

Cordey R., Pearson T., Desnos Y.-L. & Rosich-Tell B. 2004. ASAR wide-swath single-look complex products: processing and exploitation potential. In: *Proceedings of ESA Fringe 2003 Workshop, Frascati, Italy. ESA Special Publication SP-550.* European Space Agency. Accessed on the internet at http://earth.esa.int/workshops/fringe03/proceedings/ on 1 April 2011

Ezraty R., Girard-Ardhuin F. & Croizé-Fillon D. 2006. *Sea ice drift in the central Arctic using the 89 GHz brightness temperatures of the Advanced Microwave Scanning Radiometer (AMSR-E). User's Manual. Version 2.0, February 2007.* Brest: Spatial Oceanography Laboratory, French Research Institute for Exploration of the Sea.

Fieg K., Gerdes R., Fahrbach E., Beszczynska-Möller A. & Schauer U. 2010. Simulation of oceanic volume transports through Fram Strait 1995–2004. *Ocean Dynamics 60,* 491–502.

Fisher N. 1996. *Statistical analysis of circular data.* Cambridge: Cambridge University Press.

Gerdes R., Karcher M., Kauker F. & Schauer U. 2003. Causes and development of repeated Arctic Ocean warming events. *Geophysical Research Letters 30,* article no. 1980, doi: 10.1029/2003GL018080.

Girard-Ardhuin F. & Ezraty R. 2005. Validation of Arctic sea ice drift with IABP buoys. Paper presented at the Second Annual MERSEA Meeting. 29–31 March, Toulouse, France. Accessed online at http://cersat.ifremer.fr/science/sea_ice/validation_of_arctic_sea_ice_drift_with_iabp_buoys on 1 April 2011

Gordon R.L. 1996. *Acoustic Doppler current profiler. Principles of operation. A practical primer.* San Diego, CA: RD Instruments.

Harder M., Lemke P. & Hilmer M. 1998. Simulation of sea ice transport through Fram Strait: natural variability and sensitivity to forcing. *Journal of Geophysical Research—Oceans 103,* 5595–5606.

Hibler W.D.III. 1979. A dynamic thermodynamic sea ice model. *Journal of Physical Oceanography 9,* 815–846.

Jakobsson M., Macnab R., Mayer L., Anderson R., Edwards M., Hatzky J., Schenke H. & Johnson P. 2008. An improved bathymetric portrayal of the Arctic Ocean: implications for ocean modeling and geological, geophysical and oceanographic analyses. *Geophysical Research Letters 35,* L07602, doi: 10.1029/2008GL033520.

Jammalamadaka S. & Sengupta A. 2001. *Topics in circular statistics.* London: World Scientific Publishing.

Kanamitsu M., Ebisuzaki W., Woollen J., Yang S., Hnilo J., Fiorino M. & Potter G. 2002. NCEP-DOE AMIP-II reanalysis (R-2). *Bulletin of the American Meteorological Society 83,* 1631–1643.

Karcher M., Gerdes R., Kauker F. & Köberle C. 2003. Arctic warming: evolution and spreading of the 1990s warm event in the Nordic seas and the Arctic Ocean. *Journal of Geophysical Research—Oceans 108,* article no. 3034, doi: 10.1029/2001JC001265.

König Beatty C. & Holland D. 2010. Modeling landfast sea ice by adding tensile strength. *Journal of Physical Oceanography 40,* 185–198.

Kreyscher M., Harder M., Lemke P. & Flato G. 2000. Results of the Sea Ice Model Intercomparison Project: evaluation of sea ice rheology schemes for use in climate simulations. *Journal of Geophysical Research—Oceans 105,* 11299–11320.

Kwok R., Schweiger A., Rothrock D., Pang S. & Kottmeier C. 1998. Sea ice motion from satellite passive microwave imagery assessed with ERS SAR and buoy motions. *Journal of Geophysical Research—Oceans 103,* 8191–8214.

Lavergne T., Eastwood S., Teffah Z., Schyberg H. & Breivik L. 2010. Sea ice motion from low-resolution satellite sensors: an alternative method and its validation in the Arctic. *Journal of Geophysical Research—Oceans,* C10032, doi: 10.1029/2009JC005958.

Lemke P., Hibler W., Flato G., Harder M. & Kreyscher M. 1997. On the improvement of sea-ice models for climate simulations: the Sea Ice Model Intercomparison Project. *Annals of Glaciology 25,* 183–187.

Lieser J.L. 2004. *A numerical model for short-term sea ice forecasting in the Arctic. Berichte zur Polarfor- und Meeresforschung 485.* Bremerhaven: Alfred Wegener Institute for Polar and Marine Research.

Martin T. & Gerdes R. 2007. Sea ice drift variability in Arctic Ocean Model Intercomparison Project models and observations. *Journal of Geophysical Research—Oceans 112,* C04S10, doi: 10.1029/2006JC003617.

Meier W., Maslanik J. & Fowler C. 2000. Error analysis and assimilation of remotely sensed ice motion within an Arctic sea ice model. *Journal of Geophysical Research—Oceans 105,* 3339–3356.

Pacanowski R. 1995. *MOM 2 documentation, user's guide and reference manual. Technical report 3.* Princeton, NJ: Geophysical Fluid Dynamics Laboratory.

Rigor I. & Colony R. 1997. Sea-ice production and transport of pollutants in the Laptev Sea, 1979–1993. *Science of the Total Environment 202,* 89–110.

Rollenhagen K., Timmermann R., Janjic T., Schröter J. & Danilov S. 2009. Assimilation of sea ice motion in a finite-element sea ice model. *Journal of Geophysical Research—Oceans 114,* C05007, doi: 10.1029/2008JC005067.

Rosich B. & Meadows P. 2004. *Absolute calibration of ASAR level 1 products generated with PF-ASAR.* Frascati, Italy: European Space Agency.

Rothrock D. 1975. The mechanical behavior of pack ice. *Annual Review of Earth and Planetary Sciences 3,* 317–342.

Rozman P. 2009. *The role of the fast ice in an Arctic sea ice–ocean coupled model.* Master's thesis, Bremen University, Bremen, Germany.

Thorndike A. & Colony R. 1982. Sea ice motion in response to geostrophic winds. *Journal of Geophysical Research—Oceans 87,* 5845–5852.